

The radiated fields of the fundamental mode of photonic crystal fibers

Ali Dabirian,¹ Mahmood Akbari,¹ and Niels Asger Mortensen²

¹Department of Electrical Engineering, Sharif University of Technology,
Tehran, 14115-337, Iran

²MIC – Department of Micro and Nanotechnology, Technical University of Denmark,
DK-2800 Kongens Lyngby, Denmark

ali_dabirian@yahoo.com

Abstract: The six-fold rotational symmetry of photonic crystal fibers has important manifestations in the radiated fields in terms of *i*) a focusing phenomena at a finite distance from the end-facet and *ii*) the formation of low-intensity satellite peaks in the asymptotic far field. For our study, we employ a surface equivalence principle which allows us to rigorously calculate radiated fields starting from fully-vectorial simulations of the near field. Our simulations show that the focusing is maximal at a characteristic distance from the end-facet. For large-mode area fibers the typical distance is of the order $10 \times \Lambda$ with Λ being the pitch of the triangular air-hole lattice of the photonic crystal fiber.

© 2018 Optical Society of America

OCIS codes: 060.2430, 230.3990, 000.4430

References and links

1. J. C. Knight, T. A. Birks, P. S. J. Russell, and D. M. Atkin, "All-silica single-mode optical fiber with photonic crystal cladding," *Opt. Lett.* **21**, 1547–1549 (1996).
 2. T. A. Birks, J. C. Knight, and P. S. J. Russell, "Endlessly single mode photonic crystal fibre," *Opt. Lett.* **22**, 961–963 (1997).
 3. M. D. Nielsen, J. R. Folkenberg, N. A. Mortensen, and A. Bjarklev, "Bandwidth comparison of photonic crystal fibers and conventional single-mode fibers," *Opt. Express* **12**, 430 (2004). URL <http://www.opticsexpress.org/abstract.cfm?URI=OPEX-12-3-430>.
 4. J. Limpert, T. Schreiber, S. Nolte, H. Zellmer, A. Tünnermann, R. Iliev, F. Lederer, J. Broeng, G. Vienne, A. Petersson, and C. Jakobsen, "High-power air-clad large-mode-area photonic crystal fiber laser," *Opt. Express* **11**, 818–823 (2003). URL <http://www.opticsexpress.org/abstract.cfm?URI=OPEX-11-7-818>.
 5. T. F. Johnston, " M^2 concept characterizes beam quality," *Laser Focus World* **26**, 173 (1990).
 6. N. A. Mortensen, "Effective area of photonic crystal fibers," *Opt. Express* **10**, 341–348 (2002). URL <http://www.opticsexpress.org/abstract.cfm?URI=OPEX-10-7-341>.
 7. N. A. Mortensen and J. R. Folkenberg, "Near-field to far-field transition of photonic crystal fibers: symmetries and interference phenomena," *Opt. Express* **10**, 475–481 (2002). URL <http://www.opticsexpress.org/abstract.cfm?URI=OPEX-10-11-475>.
 8. C. A. Balanis, *Advanced Engineering Electromagnetic* (John Wiley & Sons, New York, 1989).
 9. E. Silberstein, P. Lalanne, J. P. Hugonin, and Q. Cao, "On the use of grating theory in integrated optics," *J. Opt. Soc. Am. A* **18**, 2865–2875 (2001).
 10. Q. Cao, P. Lalanne, and J. P. Hugonin, "Stable and efficient Bloch-mode computational method for one-dimensional grating waveguide," *J. Opt. Soc. Am. A* **19**, 335–338 (2002).
 11. J. Vučković, M. Lončar, H. Mabuchi, and A. Scherer, "Optimization of the Q Factor in photonic crystal microcavities," *IEEE J. Quantum Electron.* **38**, 850 (2002).
 12. A. K. Ghatak and K. Thyagarajan, *Introduction to Fiber Optics* (Cambridge University Press, Cambridge, 1998).
-

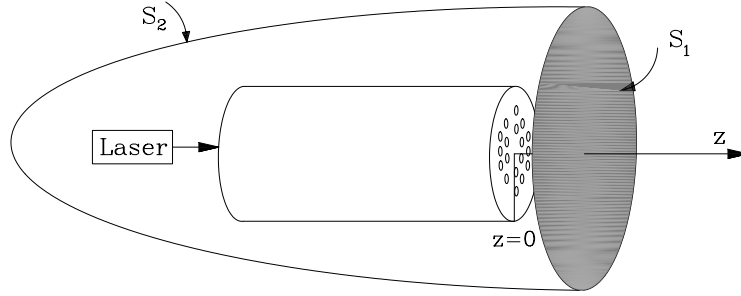


Fig. 1. Schematics of the fiber geometry and the imaginary closed surface $S = S_1 + S_2$, where S_1 is a circle parallel and close to the end-facet and S_2 is a semi-sphere concentric with S_1 .

The photonic crystal fiber [1, 2] (PCF) offers a unique opportunity for realizing broadband large-mode area (LMA) single-mode (SM) fibers [3]. In high-power laser applications the LMA property is desirable to keep the power density below the damage threshold of silica as well as to avoid non-linear phenomena and the SM property is essential for the beam quality and the ability to generate close to diffraction-limited beams. Recent studies of LMA-SM-PCF lasers have suggested that the PCF technology may indeed offer good beam quality [4] as quantified by an M -squared value [5] close to unity ($M^2 = 1$ for a Gaussian beam).

For the fundamental mode in PCFs the near and far fields have intensity distributions which are overall close to Gaussian, but with a six-fold rotational symmetry reflecting the symmetry of the air-hole lattice. For LMA-PCFs there are no significant deviations from a Gaussian distribution for intensities above the $1/e^2$ level [6] and for many practical applications the mode may be considered Gaussian. However, as studied recently the derivation from a Gaussian distribution has some important consequences [7]. In the near-field the intensity is suppressed at the locations of the air-holes and in the asymptotic far-field these suppressions manifest themselves as low-intensity satellite peaks. Furthermore, in the near field to far-field transition the intensity becomes strongly focused at a finite distance from the end-facet as can be understood by a simple Gaussian decomposition of the near field.

While the simple decomposition approach has proved very useful for the qualitative understanding of the near to far-field transition the laser applications call for a more quantitative study of the radiated field. Calculating the diffraction pattern is generally a complicated task, which involves the full solution to the elastic scattering problem at the end-facet. Here, we rigorously calculate radiated fields from the end-facet utilizing a surface equivalence principle [8].

The calculations of the modal reflectivity from the fiber end-facet is performed with a three-dimensional frequency domain modal method relying on Fourier expansion technique [9, 10]. In brief, the Fourier expansion method relies on an analytical integration of Maxwells equations along one direction (the fiber axis) and on a supercell approach in the other two transversal directions. We emphasize that for the radiated field at the surface S_1 we have treated the elastic scattering at the end-facet fully, i.e. the incident fundamental mode is partly reflected (no mode mixing for symmetry reasons) and partly radiated/transmitted. Through the surface equivalence principle, any wave-front can be considered as a source of secondary waves which add to produce distant wave-fronts according to Huygens principle.

In order to apply the surface equivalence principle, we surround the end-facet radiating fiber with an imaginary closed surface $S = S_1 + S_2$, where S_1 is a circle parallel and close to the end-facet and S_2 is a semi-sphere concentric with S_1 , see Fig. 1. Both of these surfaces are of infinite extent. By considering proper surface currents on S which are equivalent in the sense

that they yield the same field outside S , we can formally erase all the existing elements inside S and fill it with a perfect electric conducting (PEC) body. The equivalent surface electrical and magnetic currents on S are $\mathbf{J}_e(\mathbf{r}) = \hat{\mathbf{n}} \times \mathbf{H}$ and $\mathbf{M}_e(\mathbf{r}) = -\hat{\mathbf{n}} \times \mathbf{E}$, respectively, where $\hat{\mathbf{n}}$ is an outward normal to the surface S [8]. Of course, these currents radiate in the presence of the PEC and not in unbounded free-space. Because of the infinite radius of S_2 , electromagnetic fields on this surface take zero value. On S_1 electromagnetic fields are determined from near-fields. Since the S_1 surface is an infinitely extended flat PEC body we can utilize image theory to replace the conductor by image currents $-\mathbf{J}_e$ and \mathbf{M}_e . Ultimately, computation of radiated fields of an open-ended PCF is simplified to computing radiated fields of the fictitious current source $\mathbf{M}(\mathbf{r}) = 2\mathbf{M}_e(\mathbf{r}) = -2\hat{\mathbf{n}} \times \mathbf{E}$ in free-space. Calculating radiated fields of the current source can be achieved systematically through electric $\pi_e(\mathbf{r})$ and magnetic $\pi_m(\mathbf{r})$ Hertz vector potentials defined by:

$$\pi_e(\mathbf{r}) = \frac{-j}{4\pi\omega\epsilon_0} \int_S \mathbf{J}(\mathbf{r}') \frac{e^{-jk|\mathbf{r}-\mathbf{r}'|}}{|\mathbf{r}-\mathbf{r}'|} dS', \quad (1a)$$

$$\pi_m(\mathbf{r}) = \frac{-j}{4\pi\omega\mu_0} \int_S \mathbf{M}(\mathbf{r}') \frac{e^{-jk|\mathbf{r}-\mathbf{r}'|}}{|\mathbf{r}-\mathbf{r}'|} dS'. \quad (1b)$$

Employing these potentials, electric and magnetic fields are obtained by:

$$\mathbf{E}(\mathbf{r}) = (k^2 + \nabla^2)\pi_e(\mathbf{r}) - j\omega\mu_0\nabla \times \pi_m(\mathbf{r}), \quad (2a)$$

$$\mathbf{H}(\mathbf{r}) = j\omega\epsilon_0\nabla \times \pi_e(\mathbf{r}) + (k^2 + \nabla^2)\pi_m(\mathbf{r}), \quad (2b)$$

where $\omega = ck$, $k = 2\pi/\lambda$, and λ is the free-space wavelength. From Eqs. (2a) and (2b) we expect an improvement in computational time by a factor of roughly two compared to a direct use of the surface equivalence principle [11] in which both fictitious electric and magnetic surface currents exist.

We employ the described approach in a fully vectorial study of the evolution of the fundamental mode of a PCF from near-field to far-field. As an example we consider the fundamental mode in a pure-silica PCF with a normalized air-hole diameter $d/\Lambda = 0.45$ and in our simulations we utilize the scale-invariance of Maxwell's equations for a frequency-independent dielectric function. Recent experimental studies showed quite complicated interference phenomena in the near to far-field transition [7] and in particular a focusing behavior was observed at a finite distance from the end-facet. As illustrated in Fig. 2 this focusing phenomena is born out by our numerical simulation where the peak intensity of the radiation increases up to short distances from the fiber end-facet. The electric field intensity is maximal at a distance z_0 which is typically in the range $\Lambda \lesssim z_0 \lesssim 10 \times \Lambda$. At this particular distance the intensity pattern is rotated by an angle of $\pi/6$ compared to the near-field, in full agreement with the experimental observations. As the wavelength is increased relative to the pitch the diffraction by the six inner-most air holes increases and z_0 shifts closer to the end facet of the PCF. We emphasize that this interference phenomenon has no counterparts for e.g. step-index fibers with cylindrical symmetry; the focusing relies fully on the six-fold rotational symmetry of the air-hole lattice. It should also be emphasized that the phase-front is non-trivial (non-constant) in the transverse plane at z_0 and in that sense the focusing differs from that observed with a classical lens.

In Fig. 3 we show the electric field amplitude at various distances from the end-facet up to the asymptotic far-field region. The nearly hexagonal shape of the fundamental mode of the fiber (Panel A) is transformed into a nearly circular shape (Panel B) which is followed by a hexagonal shape at $z \simeq z_0$ (Panel C) where the orientation is rotated by an angle of $\pi/6$ with respect to the fiber mode at $z = 0$. This hexagonal shape expands as it propagates (Panels D and E) and then becomes close to circular again above the $1/e$ amplitude level (Panel F). As the

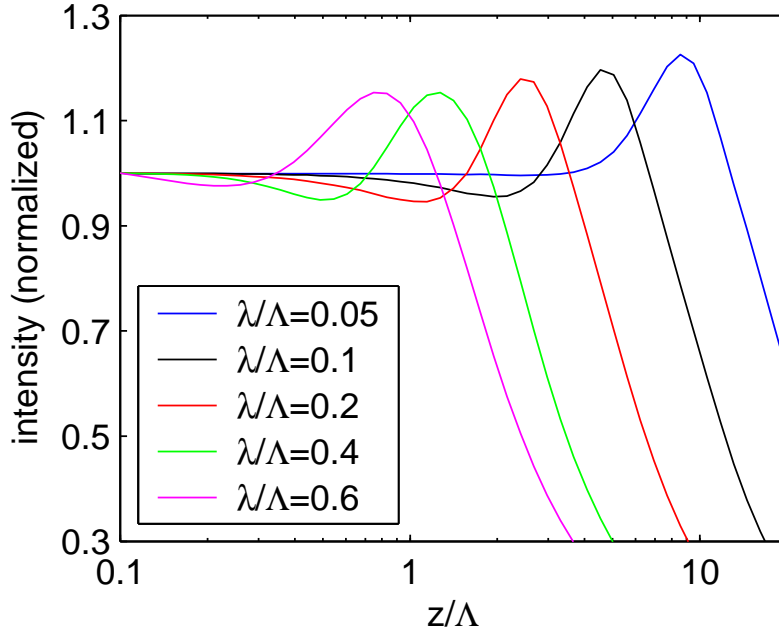


Fig. 2. Variation of the electric field intensity with distance from the end-facet ($z = 0$) at the center of fiber.

distance from the end-facet becomes larger, six satellites start emerging from the mode shape below the $1/e$ amplitude level (Panel G). Finally, for larger distances satellites appear clearly (Panel H).

As an alternative to the above rigorous approach, it is in fiber optics common to approximate the far field by a Fourier transformation of the near field [12]. Here we shall derive this expression starting from the above formalism. In the far-field limit we approximate the $|\mathbf{r} - \mathbf{r}'|$ in the denominators of Eqs. (1a) and (1b) by r and in the exponential we correspondingly approximate it by $r - \hat{\mathbf{r}} \cdot \mathbf{r}'$, where $\hat{\mathbf{r}} = \mathbf{r}/r$ is the unit radial vector of the spherical coordinate. The magnetic Hertz vector potential, Eq. (1b), then simplifies to

$$\pi_m(\mathbf{r}) \simeq \frac{-j}{4\pi\omega\mu_0} \frac{\exp(-jkr)}{r} \mathbf{N}(\theta, \phi), \quad (3)$$

where

$$\mathbf{N}(\theta, \phi) = \int_S \mathbf{M}(\mathbf{r}') e^{jk\hat{\mathbf{r}} \cdot \mathbf{r}'} dS', \quad (4)$$

with θ and ϕ being the polar and azimuthal angles, respectively, and $\mathbf{r} = r\hat{\mathbf{r}} + \phi\hat{\boldsymbol{\phi}} + \theta\hat{\boldsymbol{\theta}}$. The electric field now becomes

$$\mathbf{E}(\mathbf{r}) \simeq \frac{-1}{4\pi} \frac{e^{-jkr}}{r} (-jk)(\hat{\mathbf{r}} \times \mathbf{N}). \quad (5)$$

We will consider small angles θ of divergence so that $\hat{\mathbf{r}} \times \mathbf{M} = -M_y\hat{\mathbf{x}} + M_x\hat{\mathbf{y}} + \mathcal{O}(\theta)$ by which Eq. (5) simplifies to

$$\mathbf{E}(\mathbf{r}) \simeq \frac{jk}{2\pi} \frac{e^{-jkr}}{r} \int_S \mathbf{E}_t(x', y', z' = 0) \times \exp[jk(x' \sin\theta \cos\phi + y' \sin\theta \sin\phi)] dS', \quad (6)$$

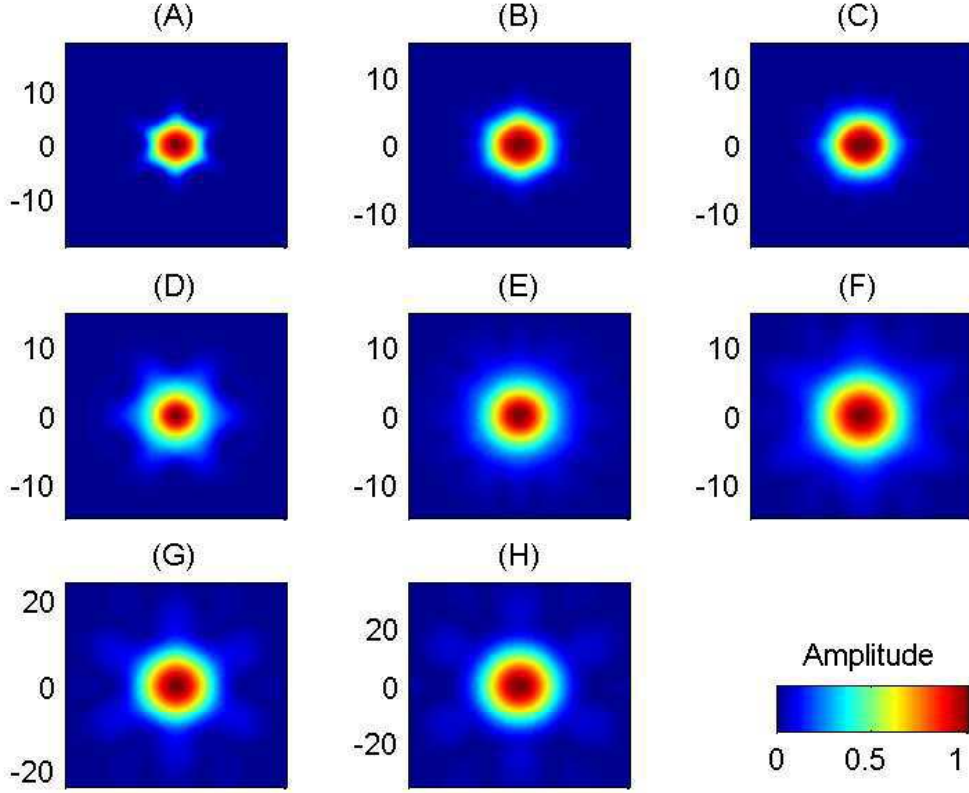


Fig. 3. Electric field amplitudes at distances z from the end-facet varying from $z = 0$ (Panel A) to $z = 12 \times \Lambda$ (Panel H).

with the subscript t indicating the transverse component. The integral is nothing but a two-dimensional Fourier transform of the near-field corresponding to the overlap of the near field with a free-space plane-wave.

Fig. 4 shows a plot of the asymptotic far-field intensity, including results of the rigorous surface-equivalence principle as well as the approximate far-field calculated from Eq. (6). The far-field pattern is computed for $\lambda/\Lambda = 0.1$ at a distance of $1000 \times \Lambda$ from the end-facet, which is far from the starting point of the Fraunhofer region. For an extended source of electromagnetic radiation, the Fraunhofer region appears at a characteristic distance $2D^2/\lambda$ from the source where the parameter D is defined by the maximum linear dimension of the source. For a PCF $D \sim 2\Lambda$, so Fraunhofer region sets in around $80 \times \Lambda$. The inset shows a contour plot of the far-field intensity calculated with the rigorous surface-equivalence principle. We observe six low-intensity satellite peaks as well as further high-order diffraction peaks, in full agreement with experimental observations [1, 7]. As seen, the approximate results of Eq. (6) are in qualitative agreement with the full numerical solution, and it is only in the sub- $1/e^2$ intensity regime that we observe quantitative deviations. This suggests that Eq. (6) could be a good starting point for numerical calculations of the NA and the M-squared value for LMA PCFs, which we will report elsewhere.

In conclusion we have used a surface equivalence principle to rigorously calculate radiated fields starting from fully-vectorial simulations of the near field. Our simulations have revealed

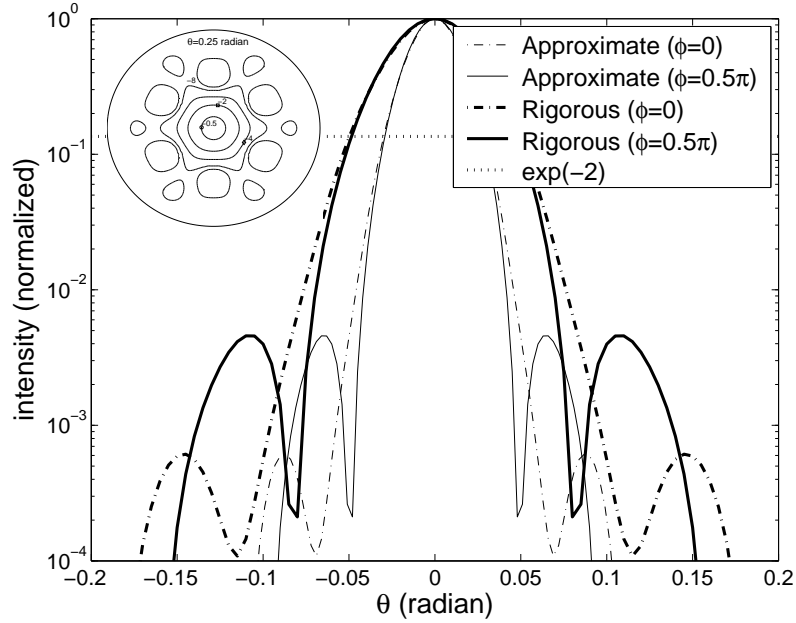


Fig. 4. Asymptotic far-field intensities calculated by the rigorous approach as well as the approximate expression, Eq. (6), along the high-symmetry directions $\phi = 0$ and $\phi = \pi/2$. The inset shows the corresponding full contour plot obtained with the rigorous approach.

a focusing behavior which is maximal at a characteristic distance, of the order $10 \times \Lambda$ from the end-facet. In the far-field limit we have shown how qualitative and to some degree also quantitative insight may be gained from simple two-dimensional Fourier transforms of the near-field.

We thank J. R. Folkenberg and P. M. W. Skovgaard (both with Crystal Fibre A/S) for stimulating discussions. N. A. M. is supported by The Danish Technical Research Council (Grant No. 26-03-0073).